



Cite this: *Phys. Chem. Chem. Phys.*, 2019, 21, 8445

Atmospheric oxidation reactions of imidazole initiated by hydroxyl radicals: kinetics and mechanism of reactions and atmospheric implications†

Zahra Safaei, ^a Abolfazl Shiroudi, *^b Ehsan Zahedi ^c and Mika Sillanpää ^a

The atmospheric oxidation mechanism of imidazole initiated by hydroxyl radicals is investigated via OH-addition and H-abstraction pathways by quantum chemistry calculations at the M06-2X/aug-cc-pVTZ level of theory coupled with reaction kinetics calculations using statistical Rice–Ramsperger–Kassel–Marcus (RRKM) theory and transition state theory (TST). It was found that OH addition proceeds more rapidly than H-abstraction by several orders of magnitude. Moreover, H-abstraction reactions with submerged barriers exhibit positive temperature dependence. Effects of reaction temperature and pressure on the reaction between imidazole and OH radicals are studied by means of RRKM calculations. Effective rate coefficients involve two-step mechanisms. According to the experiment, the obtained branching ratios show that the kinetically most efficient process corresponds to OH addition onto a carbon atom which is adjacent to a nitrogen atom having a lower energy barrier. These ratios also reveal that the regioselectivity of the oxidation reaction decreases with increasing temperatures and decreasing pressures. Because of negative activation energies, pressures larger than 100 bar are required to reach the high pressure limit. The atmospheric lifetime of imidazole in the presence of OH radicals is estimated to be ~4.74 days, based on the calculated overall kinetic rate constant of $1.22 \times 10^{-12} \text{ cm}^3 \text{ molecule}^{-1} \text{ s}^{-1}$ at a pressure of 1 bar and nearly ambient temperature. NBO analysis demonstrates that the calculated energy barriers are dictated by charge transfer effects and aromaticity changes because of the delocalization of nitrogen lone pairs to empty π^* orbitals.

Received 31st January 2019,
Accepted 19th March 2019

DOI: 10.1039/c9cp00632j

rsc.li/pccp

1. Introduction

The aromatic heterocycle imidazole is widespread in organic compounds. Imidazole plays an important role in biochemical processes because of its special acid–base characteristics. The side chain of histidine contains a weakly basic imidazole group that is a versatile catalyst; it is a strong Lewis base, besides a

nucleophile, and it is a Brønsted acid in its protonated form. Accordingly, some histidine residues are essential for the activity of proteins such as hemoglobin, carbonic anhydrase, adenosine deaminase, triose phosphate isomerase, serine proteases, chymotrypsin, *etc*. Moreover, two nitrogenous bases found in nucleotides, adenine and guanine, are derivatives of purine, a heterocycle consisting of fused pyrimidine and imidazole rings. Nucleotides are building blocks of nucleic acids and coenzymes with diverse functions.^{1–3} It is well-known that the reactions of the OH radicals with aromatic and heterocyclic compounds are much favored.

In the reaction between aromatic compounds and OH radicals, an addition of hydroxyl radicals and the consequent unimolecular decay of the [aromatic-OH][•] adduct back to the isolated reactants is assumed to be the main reaction path.⁴ Since only some investigations have been carried out on the reaction between aromatic heterocyclic compounds and OH radicals,^{5–12} Witte and Zetzsch¹³ have tried to get further information on the oxidation reaction mechanism of imidazole initiated by OH radicals in the gas phase. In order to consider the temperature dependence, a flash photolysis resonance fluorescence (FP-RF) technique over the temperature range 297–447 K has been used in this study. Biexponential decays of OH radicals are found in the presence of

^a Department of Green Chemistry, LUT University, Sammonkatu 12, FI-50130 Mikkeli, Finland

^b Young Researchers and Elite Club, East Tehran Branch, Islamic Azad University, Tehran, Iran. E-mail: abolfazl.shiroudi@iauet.ac.ir

^c Chemistry Department, Shahrood Branch, Islamic Azad University, Shahrood, Iran

† Electronic supplementary information (ESI) available: Supplementary data (Tables S1–S3) associated with this article can be found, in the online version. Table S1: kinetic rate constants for the reactions involved in the reaction pathways 1–3 by means of RRKM theory at different pressures and temperatures, according to the computed M06-2X energy profiles; Table S2: kinetic rate constants (*k*) for OH attack onto C₂, C₄, and C₅ positions of imidazole for different addition products by means of TST (*P* = 1 bar) (*x* = 2, 3); Table S3: effective bimolecular rate constants (cm³ molecule⁻¹ s⁻¹), branching ratios (%) and regioselectivity for the pathways 1–3 (*x* = 1, 2) at different pressures and temperatures, using RRKM theory, and according to the computed M06-2X energy profiles. See DOI: 10.1039/c9cp00632j



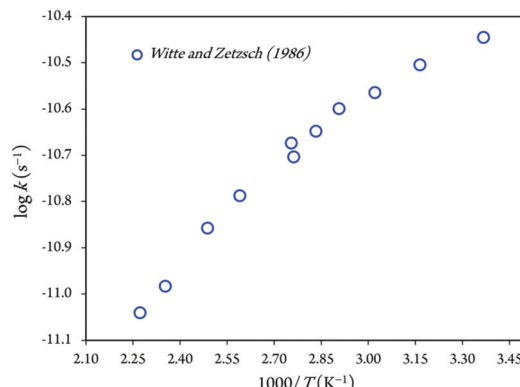


Fig. 1 Arrhenius plot for the kinetic rate constant of reaction between imidazole and OH radicals.²⁹

imidazole at a pressure of 133 mbar with argon (Ar) as an inert gas over the temperature range from 353 to 425 K. The reaction between imidazole and OH radicals shows negative activation energy, which indicates an electrophilic addition of OH to the imidazole. The ratio estimation for the amounts of biexponential decay curve yield equilibrium constants, and therefore kinetic rate constants for the unimolecular decay of the [imidazole-OH][•] adducts leading back to the isolated reactants. Using activation energy, it is possible to derive the bond dissociation energies of the [imidazole-OH][•] adducts forming back hydroxyl radicals.

An Arrhenius plot of the rate coefficients measured at the temperature range from 297 to 440 K is shown in Fig. 1. The kinetic rate coefficient between imidazole and hydroxyl radicals shows negative temperature dependences over the temperature range 297–440 K, which is equivalent to Arrhenius activation energies of $-(1847.91 \pm 158.96) \text{ cal mol}^{-1}$.¹³ Hence, the least-square fit of the experimental rate constants yields as follows:^{13–15}

$$k_{\text{forward}} = (1.7 \pm 0.4) \times 10^{-12} \exp[(930 \pm 80)/T] \text{ cm}^3 \text{ molecule}^{-1} \text{ s}^{-1}$$

$$k_{\text{reverse}} = 5 \times 10^9 \exp[-(7800 \pm 700)/T] \text{ s}^{-1}$$

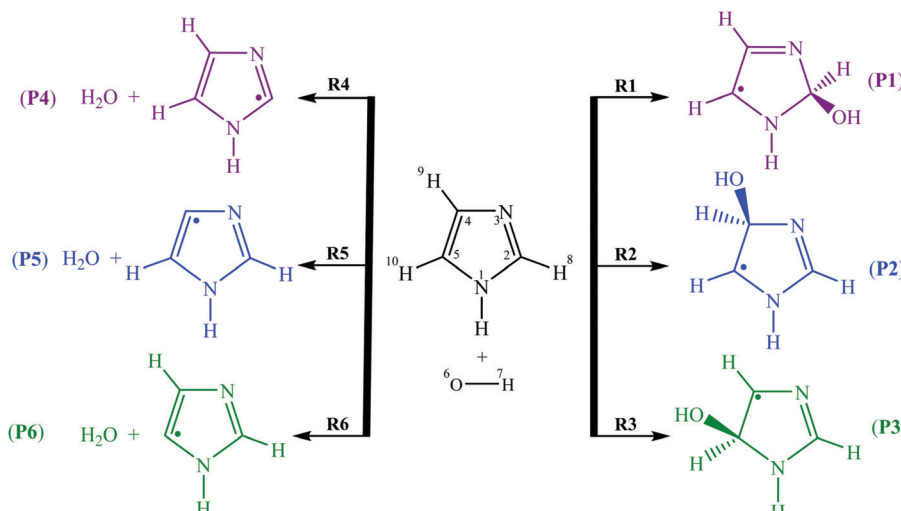


Fig. 2 Oxidation reactions between imidazole and hydroxyl radicals.

The kinetic rate coefficient decreases with increasing temperature over the temperature range from 297 to 440 K,¹⁶ confirming negative activation energies. The corresponding values vary from $(35.9 \pm 3.3) \times 10^{-12}$ to $(9.1 \pm 1.1) \times 10^{-12} \text{ cm}^3 \text{ molecule}^{-1} \text{ s}^{-1}$.

Experiments show that hydroxyl radicals react with imidazoles by addition at a carbon adjacent to the nitrogen (C_2 or C_5 positions).^{17,18} The oxidation reaction of imidazole (**I**) initiated by hydroxyl radicals might yield three possible adducts, *i.e.*, the 2-hydroxyimidazolyl (**I2-OH[•]**), 4-hydroxyimidazolyl (**I4-OH[•]**), and 5-hydroxyimidazolyl (**I5-OH[•]**) radicals. Nevertheless, electron spin resonance (ESR) measurements and experimental data¹⁷ as well as a theoretical study by Llano and Eriksson³ revealed that in neutral and alkaline ($\text{pH} = 9\text{--}10$) aqueous solutions, hydroxyl radicals exactly add on the carbon adjacent to the nitrogen (C_5 position) and in acidic media ($\text{pH} = 2$), to the same position leading to the 5-adduct.^{17–19} In spite of the site specificity, **I2-OH[•]** adducts are energetically more favored by $\sim 4 \text{ kcal mol}^{-1}$ than **I5-OH[•]** adducts.

To explain the difference of the kinetic rate constants, six various reactions (1)–(6) were proposed for the oxidation of imidazole by OH radicals in the gas phase (Fig. 2) *via* H-abstraction and OH-addition reactions. In this study, the main purpose is to investigate theoretically these pathways, upon the assumption of a two-step mechanism. To our knowledge, the present work is the first one, which investigates the oxidation mechanisms between imidazole and hydroxyl radicals under experimental conditions:

– OH-addition pathway through attack of hydroxyl radicals onto C_2 , C_4 and C_5 atoms yields the products **P1–P3**, respectively.

– H-abstraction pathway *via* attack of OH radicals bonded to C_2 , C_4 and C_5 atoms gives the products **P4–P6**, respectively.

In proportion to the hypothesis of the first reversible addition step, the negative energy barrier of this pathway at 298 K points out that the main pathway of the [imidazole-OH][•] adducts is loss of OH radicals to regenerate the isolated reactants.⁶ Upon investigating the regioselectivity of OH-addition pathways on imidazole under an inert atmosphere, it was observed that the pathways 1 and 3 associated with the OH addition onto C_2 and C_5 atoms dominate over hydroxyl radical addition onto the C_4 atom (pathway 2).

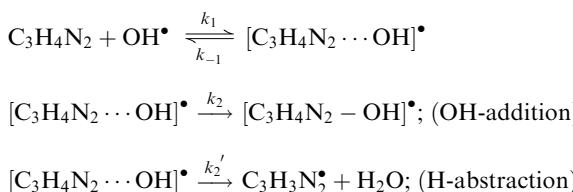
The obtained M06-2X results will be investigated concerning natural bond orbital (NBO) occupancies,^{25,26} nucleus independent chemical shift (NICS) indices of aromaticity,^{20–24} and the nature of electron donor–acceptor interactions for the sake of chemical insights. In this work, we studied the kinetics of oxidation of imidazole. *Ab initio* calculations of the transition state theory (TST) as well as RRKM theory were used to determine the kinetic rate coefficients *via* H-abstraction and OH-addition pathways over the temperatures ranging from 297 to 440 K using the M06-2X method to explore the intrinsic insight of the imidazole in the gas-phase which can provide important information for the experimental mechanism investigation. Finally, our obtained theoretical results were compared with experimental data and the results from preceding theoretical studies.

2. Theory and computational details

All the electronic structure calculations were achieved using the Gaussian 09 program.²⁷ The geometrical structures of the stationary points are optimized and vibrational frequencies are calculated at the M06-2X/aug-cc-pVTZ theoretical level^{28,29} which was found to be a suitable exchange–correlation functional for thermochemical and kinetics calculations.²⁹ Zero-point vibrational energies (ZPVE) were calculated from the M06-2X harmonic frequencies with the scaling factor of 0.971.^{30,47}

The intrinsic reaction coordinates (IRC)³¹ for both directions (forward and reverse) were also performed in order to confirm that the transition state structure properly connects reactants and products.³² IRC calculation uses 30 points in the forward direction and 30 points in the reverse direction, in steps of 0.1 amu^{1/2} Bohr along the path. The NICS values are achieved by implementation of the gauge-independent atomic orbital (GIAO) method³³ to determine the diamagnetic ring current intensity on the optimized geometries of all stationary points along the studied reaction pathways. Schleyer *et al.*²³ state that there is a good linear relationship between the geometric, energetic, and magnetic properties in the organic molecules. The magnetic shielding tensor is calculated for Bq ghost atoms which located at the ring critical point, the point of lowest density in the ring plane to yield NICS(0) values.^{34–36} The NICS(0) values calculated at the center of the ring were influenced by σ -bonds, whereas the NICS(1) values calculated at 1 Å above the plane were more affected by the π -system which is considered to better reflect the π -electron effects than NICS(0).^{22,23}

The oxidation reaction of imidazole by hydroxyl radicals was analyzed consistent with the scheme³⁷ that is expected; the pathway takes place consistent with the two-step reaction mechanism³⁸ including first the fast pre-equilibrium between the reactants ($\text{C}_3\text{H}_4\text{N}_2 + \text{OH}^\bullet$) and a prereactive complex $[\text{C}_3\text{H}_4\text{N}_2 \cdot \cdot \text{OH}]^\bullet$ (IM) leading to the related products as follows:



where k_1 and k_{-1} are the forward and backward rate constants for the first step, and k_2 and k_2' correspond to the second step. The rate coefficient for the overall reaction (k_{eff}) is given by:^{37,39}

$$k_{\text{eff}} = K_c k_2 \quad (1)$$

where $K_c = k_1/k_{-1}$ is the equilibrium constant for fast pre-equilibrium between the isolated reactants and the pre-reactive complex. In the high-pressure limit (TST), the unimolecular rate coefficient can be obtained as follows

$$k_2 = \kappa(T) \times \frac{\sigma k_B T}{h} \times \frac{Q_{\text{TS}}}{Q_{\text{IM}}} \times \exp[-(E_{\text{TS}} - E_{\text{IM}})/RT] \quad (2)$$

where σ is the reaction path degeneracy, h and k_B represent the Planck's and Boltzmann's constants, respectively, and R is the ideal gas constant. Q_{IM} and Q_{TS} represent the total molecular partition functions for the pre-reactive complex (IM) and transition state (TS) related to the unimolecular reaction (step 2), respectively. Furthermore, E_{IM} and E_{TS} are consistent with energies, including M06-2X estimates for zero-point vibrational contributions, and $\kappa(T)$ represents the tunneling correction factor which is calculated using the Wigner model.^{40,41}

$$\kappa_{\text{Wigner}}(T) = 1 + \frac{1}{24} [h \text{Im}(v_i)/k_B T]^2 \quad (3)$$

where $\text{Im}(v_i)$ is the imaginary vibrational frequency of the relevant transition state.

The high-pressure limit kinetic rate coefficients for unimolecular (k_{uni} , in s^{-1}) and bimolecular (k_b , in $\text{cm}^3 \text{molecule}^{-1} \text{s}^{-1}$) reactions using TST are given by:^{42,43}

$$k_b = \kappa(T) \times \frac{\sigma k_B T}{h} \times \frac{Q_{\text{TS}}}{Q_A \cdot Q_B} \times \frac{V_m(T)}{N_{\text{Av}}} \times \exp(-\Delta E_0/RT) \quad (4)$$

$$k_{\text{uni}} = \kappa(T) \times \frac{\sigma k_B T}{h} \times \frac{Q_{\text{TS}}}{Q_R} \times \exp(-\Delta E_0/RT) \quad (5)$$

where Q_A , Q_B , and Q_{TS} are the partition functions for the isolated reactants (A and B), and transition state related to the unimolecular reaction (step 2), respectively.

In the oxidation of benzene initiated by OH radicals, there are some unimolecular reactions which might not reach their high-pressure limits under typical atmospheric conditions,⁴⁴ though the resulting product yields from RRKM theory and high-pressure limit agreed excellently. Therefore to check the validity of the high-pressure limit in imidazole oxidation, RRKM calculations were carried out for the oxidation of imidazole by OH radicals.

The energy-dependent microcanonical rate coefficients, $k(E)$ for the unimolecular reaction according to the RRKM theory is given by:⁴²

$$k(E) = \frac{\sigma G^\dagger(E - E_0)}{hN(E)} \quad (6)$$

where $N(E)$ is the density of states for the activated molecule at an energy E , and $G^\dagger(E - E_0)$ is the sum of states of the transition state.⁴⁵

Kinetic rate constants by means of TST and RRKM theories for the studied pathways were obtained using the KiSTheLP program.⁴⁶ It is worth mentioning that every collision deactivates the



molecule with $\omega = \beta_c \cdot Z_{\text{LJ}} \cdot [M]$, which is consistent with the effective collision frequency ω , along with the total gas concentration $[M]$, the collisional efficiency β_c , and the Lennard-Jones (LJ) collision frequency Z_{LJ} that was computed from the LJ parameters. The employed Lennard-Jones potential parameters (σ and ε/k_B) for $[\text{C}_3\text{H}_4\text{N}_2\text{-OH}]^\bullet$ adducts and argon (as diluent gas) are equal to ($\sigma = 4.8 \text{ \AA}$ and $\varepsilon/k_B = 492.7 \text{ K}$)⁴⁸ and ($\sigma = 3.465 \text{ \AA}$ and $\varepsilon/k_B = 113.5 \text{ K}$),⁴⁹ respectively.

3. Result and discussion

3.1. The reaction of imidazole with OH radicals

The reactions between imidazole and OH radicals involve two kinds of reaction pathways:

(1) Attack of hydroxyl radicals onto the C₂, C₄, and C₅ positions.

(2) Abstraction of hydrogen bonded to the C₂, C₄, and C₅ atoms (H abstraction from C₂-H₈, C₄-H₉, and C₅-H₁₀ bonds).

In line with a study by Alvarez-Idaboy *et al.*,⁵⁰ such a pre-reactive intermediate complex **IM** is a common feature in reactions between radical species and unsaturated molecules, which finds its origin in long range Coulomb interactions between the reactant molecules.⁵¹

3.1.1. Addition of hydroxyl radicals to imidazole. Two carbon atoms (C₄ and C₅ positions) in the C₄=C₅ bond of imidazole are not equivalent; thus, three different $[\text{C}_3\text{H}_4\text{N}_2\text{-OH}]^\bullet$ energized adducts (**P1-P3**) can be formed *via* addition of hydroxyl radicals onto the C₂, C₄, and C₅ positions, respectively, as depicted in Fig. 2. Under atmospheric conditions, the $[\text{C}_3\text{H}_4\text{N}_2\text{-OH}]^\bullet$ energized adducts could easily further react with oxygen molecules, and form intermediate $[\text{C}_3\text{H}_4\text{N}_2\text{-OH-O}_2]^\bullet$ radicals, transition states (**TS1-TS3**) for the three OH-additions and confirmed by the intrinsic reaction coordinate (IRC) approach. The reaction energies and energy barriers, as well as thermodynamical parameters,

are calculated at the M06-2X/aug-cc-pVTZ level of theory for hydroxyl radical attacks onto C₂, C₄, and C₅ positions of imidazole and are shown in Table 1.

The hydroxyl radicals attack on the imidazole ring to form two prereactive intermediates **IM1** and **IMx** ($x = 2,3$) for pathways **1-3**. In **IM1** and **IMx** ($x = 2,3$), the lengths of the C₂-O₆, C₄-O₆, and C₅-O₆ bonds are 2.542, 2.555 and 2.847 Å, respectively. The **IM1** and **IMx** ($x = 2,3$) prereactive complexes are located at 4.47 and 4.0 kcal mol⁻¹ under the total energy of imidazole and OH radicals (as the isolated reactants), respectively. The energy barriers (**IM1** → **TS1** or **IMx** → **TS2/TS3**) encountered along the pathways **1-3** amount to 2.94, 4.70, and 1.03 kcal mol⁻¹, respectively. Two isomerization processes are identified from the **IM1** and **IMx** ($x = 2,3$): the oxidation process to product **P1** *via* the transition state **TS1**, and the reaction between imidazole and OH radicals to produce pre-reactive intermediate **IMx** ($x = 2,3$) *via* the transition states **TS2** and **TS3**.

In line with experimental data,¹³⁻¹⁵ all our calculations identify the **TS3** structure (as the lowest transition state) on reaction (3), which is located at 2.97 kcal mol⁻¹ under the reactants. The **TS1** structure on reaction (1) is found at 1.53 kcal mol⁻¹ under the isolated reactants while the **TS2** structure on reaction (2) is located at 0.71 kcal mol⁻¹ above the isolated reactants. The barrier height for pathway 3 is therefore lower by 1.44 and 3.67 kcal mol⁻¹ than that for reactions (1) and (2), respectively (Table 1). This difference in energy barriers for the reactions R + OH[•] → P_i, $i = 1-3$ shows that the production of product **P3** species *via* OH attack at the C₅ position will be kinetically favored over the production of **P1** and **P2** species (through OH attack onto C₂ and C₄ positions, respectively).

The obtained results indicate that all considered reactions (1)-(3) are extremely exoergic processes ($\Delta G < 0$), and extremely exothermic processes ($\Delta H \approx -28.56$, -18.45 , and -25.92 kcal mol⁻¹, respectively) at $P = 1$ bar and $T = 298$ K. Obviously, it is formation of product **P1** (OH attack at the C₂ position), which will also be

Table 1 The relative total reaction and activated energies (in kcal mol⁻¹), as well as activation entropies (in cal mol⁻¹ K⁻¹) for all the reactions between imidazole and hydroxyl radicals at the M062X/aug-cc-pVTZ level. ($T = 298$ K, $P = 1$ atm)

Species	Parameters					
	$\Delta E_{0\text{K}}$	$\Delta H_{298\text{K}}^\circ$	$\Delta G_{298\text{K}}^\circ$	$\Delta E_{0\text{K}}^\dagger$	$\Delta H_{298\text{K}}^{\dagger\ddagger}$	$\Delta G_{298\text{K}}^{\dagger\ddagger}$
Imidazole + OH [•]	0.000	0.000	0.000			
IM1 [C ₂ position]	-4.472	-4.725	2.703			
IMx ($x = 2,3$)[C ₄ & C ₅ positions]	-3.996	-4.209	2.708			
OH-Addition pathways: [R-OH][•]						
P1 (2-hydroxyimidazolyl radical)	-27.657	-28.559	-19.081			
P2 (4-hydroxyimidazolyl radical)	-17.607	-18.445	-8.993			
P3 (5-hydroxyimidazolyl radical)	-24.962	-25.921	-16.303			
TS1 [C ₂ position]				-1.529	-2.449	6.919
TS2 [C ₄ position]				0.703	-0.230	9.219
TS3 [C ₅ position]				-2.966	-3.801	5.313
H-Abstraction pathways: [R][•] + H₂O						
P4 (2-dehydroimidazolyl + H ₂ O)	-1.814	-1.522	-2.621			
P5 (4-dehydroimidazolyl + H ₂ O)	-1.681	-1.414	-2.469			
P6 (5-dehydroimidazolyl + H ₂ O)	1.748	2.030	0.944			
TS4 [C ₂ position]				6.075	5.555	13.665
TS5 [C ₄ position]				5.856	5.301	13.577
TS6 [C ₅ position]				7.605	7.039	15.358



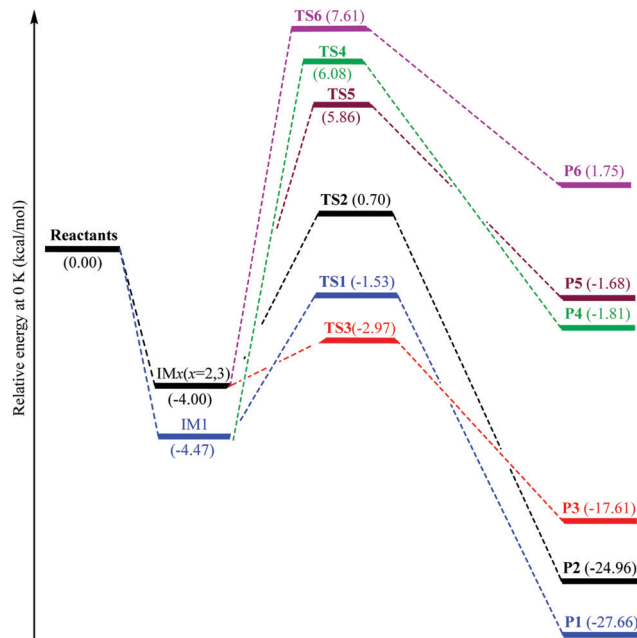


Fig. 3 Energy profiles of the H-abstraction and OH-addition reactions.

thermodynamically favored (see Fig. 3), because the reaction is strongly exoergic ($\Delta G = -19.08 \text{ kcal mol}^{-1}$) and strongly exothermic ($\Delta H = -28.56 \text{ kcal mol}^{-1}$).

The transition states **TS1**–**TS3** are considered by nucleus independent chemical shifts equal to -17.41 , -9.82 and -19.01 , respectively. Obviously, the more noticeable aromatic nature of the **TS3** structure describes its higher stability, compared with the **TS1** and **TS2** ones. Furthermore, the lesser energy of intermediate **IM1** compared with **IMx** ($x = 2,3$) reveals the more noticeable aromatic nature of the former pre-reactive molecular complex: indeed, the **IM1** and **IMx** intermediates are characterized by NICS indices equal to -12.25 and -11.77 , respectively.

3.1.2. Hydrogen abstraction pathways. Schematic potential energy diagram of the hydrogen abstraction reactions (4)–(6) is given in Fig. 3. There are three types of hydrogen in imidazole, which shows that three possible oxidation reactions could be defined.

According to the M06-2X data, two prereactive intermediates **IM1** and **IMx** ($x = 2,3$) are characterized by $\text{H}_8\text{--O}_6$, $\text{H}_9\text{--O}_6$, and $\text{H}_{10}\text{--O}_6$ bond distances equal to 2.639 , 2.722 , and 3.253 \AA , respectively. Proceeding further on reactions (1)–(3), the hydrogen H_8 , H_9 or H_{10} abstraction *via* the transition states **TS4**, **TS5**, and **TS6** requires activation energies of 6.07 , 5.86 , and $7.61 \text{ kcal mol}^{-1}$ corresponding to the isolated reactants energies (Fig. 3), respectively.

The breaking C–H bond length is elongated by ~ 15.7 – 18.3 \AA (0.17 – 0.20 \AA in absolute value) at the level of the transition states **TS4**, **TS5** and **TS6**, compared with the equilibrium structure. On the other hand, the forming O–H bond distance is larger than in H_2O . The elongation of the O–H bond in the **TS4**, **TS5**, and **TS6** structures is of the order of ~ 24.3 – 27.5% (0.23 – 0.27 \AA in absolute value) compared with the latter. The optimized structures show that the relative elongation of the C–H bond is less than that of the forming O–H bond, which shows that the **TS4**, **TS5**, and **TS6**

structures are closer to the reactants than the associated products, which is in proportion to Hammond's principle.⁵²

According to the characteristic transition states, the obtained results at ambient temperature and pressure show that the chemical pathways for **4** and **5** are found to be exothermic ($\Delta H < 0$) as well as exoergic ($\Delta G < 0$) processes while the pathway for **6** is found to be an endothermic ($\Delta H > 0$) as well as endoergic ($\Delta G > 0$) process. Because pathway **4** is exoergic ($\Delta G = -2.62 \text{ kcal mol}^{-1}$) and exothermic ($\Delta H = -1.52 \text{ kcal mol}^{-1}$), it is clear that the formation of **P4** species will be thermodynamically stable. Addition of hydroxyl radicals onto the H atom bonded to the carbon C_2 has the lowest Gibbs energy barriers ($\Delta G_{298\text{K}}^{\ddagger} = -16.303 \text{ kcal mol}^{-1}$).

In proportion to the experimental activation energy of $(-840 \pm 30) \text{ cal mol}^{-1}$ for oxidation of imidazole by OH radicals, the corresponding activation energy of these reactions (4)–(6) is 5.86 to $7.61 \text{ kcal mol}^{-1}$ above the isolated reactants. The obtained energy barriers for the studied reactions $\text{R} + \text{OH}^{\bullet} \rightarrow \text{P}_i$ ($i = 4$ – 6) show that the formation of **P5** species can be obtained by removal of a hydrogen atom bonded to the C_4 atom leading to a H_2O molecule and that 4-dehydroimidazolyl radical formation is kinetically favorable over the production of **P4** and **P6** species. The transition state **TS5** on pathway **5** is the lowest transition state, which is located at $5.86 \text{ kcal mol}^{-1}$ above the isolated reactants. The transition states **TS4** and **TS6** on reaction pathways **4** and **6** are located at 6.08 and $7.61 \text{ kcal mol}^{-1}$ above the isolated reactants, respectively. The barrier height for reaction (5) is therefore less by 0.22 and $1.75 \text{ kcal mol}^{-1}$ than the activation energy for reactions (4) and (6), respectively (Table 1).

3.1.3. Comparison of OH-addition and hydrogen abstraction pathways. All energy barrier heights of the pathways **4**–**6** are higher than those for pathways **1**–**3**. Three pathways **P4**–**P6** were found and correspond to the H_8 , H_9 and H_{10} abstraction pathways with the Gibbs free activation energies of 13.67 , 13.58 , and $15.36 \text{ kcal mol}^{-1}$ for the production of **P4**, **P5**, and **P6**, respectively. Noticeably, production of **P4** species dominated. As can be seen from Fig. 3 and Table 1, the differences in reaction energies for both the H abstraction and OH addition reactions show that the production of **P1**–**P3** species was thermodynamically favorable. Among the **P1**–**P3** species, the production of **P1** species [OH attack onto C_2 atom] was the most favorable reaction among the other products, since pathway **1** is strongly exoergic ($\Delta G = -19.08 \text{ kcal mol}^{-1}$) and strongly exothermic ($\Delta H = -28.56 \text{ kcal mol}^{-1}$). With reaction energies -17.61 to $-27.66 \text{ kcal mol}^{-1}$, OH-addition pathways **1**–**3** seem to be the rather strongly exothermic chemical reactions, while H-abstraction pathways **4**–**6** appear to be exothermic for pathways **4** and **5** (-1.41 to $-1.52 \text{ kcal mol}^{-1}$) and endothermic for reaction (6) ($\Delta H = 2.03 \text{ kcal mol}^{-1}$), with the reaction energies -1.81 to $1.75 \text{ kcal mol}^{-1}$.

We can see from Table 1 that oxidation processes *via* OH-addition reactions have negative Gibbs free energy of reaction ΔG_r which indicates that OH attacks onto different carbon atoms (C_2 , C_4 , and C_5) are thermodynamically spontaneous processes. Moreover, the hydroxyl radical addition occurring



at the C₂ position is thermodynamically the most favorable ($\Delta E_{0K} = -27.66$ kcal mol⁻¹), followed by addition onto the C₅ atom, and hydroxyl radical addition bonded to the C₅ position leading to a H₂O molecule and the related radical is the most unfavorable ($\Delta E_{0K} = 1.75$ kcal mol⁻¹). Instead, from the kinetic viewpoint, addition onto the C₅ atom has the lowest Gibbs free activation energy ($\Delta G^\ddagger = 5.31$ kcal mol⁻¹), followed by addition occurring at the C₂ position, while OH addition occurring at the C₅ position for the H-abstraction pathways has the highest ΔG^\ddagger value ($\Delta G^\ddagger = 15.36$ kcal mol⁻¹).

The energy barriers from the OH-addition processes (1–3) are lower than those from the H-abstraction pathways (4–6) by ~ 10.57 kcal mol⁻¹ for reactions between imidazole and OH radicals (ΔG_{298K}^\ddagger , 6.92 vs. 13.67 kcal mol⁻¹ for C₂ position, ΔG_{298K}^\ddagger , 9.22 vs. 13.58 kcal mol⁻¹ for C₄ atom and 5.31 vs. 15.36 kcal mol⁻¹ for C₅ position). Accordingly, the hydroxyl addition pathways are more important than the hydrogen atom abstraction processes. Evidently, the process reactions *via* OH-addition pathways are faster than the consistently H-abstraction pathways, as they involve noticeably lower activation energies (Table 1). Thus, from a thermodynamic viewpoint, OH addition pathways 1–3 are favored for the oxidation reaction. The obtained results show that **P1–P3** species can be obtained from pathways 1–3 and are important intermediates produced in the processes. The products **P1–P3** are activated radicals and can further react with the global oxygen molecules to form the related organic peroxy radicals in the atmosphere.

Furthermore, as can be seen in Table 1, the difference in activation energies shows that the production of **P1–P3** species related to the OH addition onto C₂, C₄, and C₅ positions will be kinetically the most favorable compared to the other products [P4–P6]. Among the reactions (1)–(3) leading to products **P1–P3**,

the supplied data demonstrate that the most favorable process is OH[•] attack onto the C₅ position from a kinetic viewpoint. The predicted Gibbs free activation energies are 6.92, 9.22, 5.31, 13.67, 13.58, and 15.36 kcal mol⁻¹ for the reactions (1)–(6), respectively. Obviously, formation reactions of (1)–(3) related to the OH attack onto different positions on the ring (C₂, C₄, and C₅) dominate. Therefore in the kinetic section, we only focus on the OH-addition pathways.

Addition of OH radicals to the hydrogen bonded C₂ and C₄ atoms is exothermic by -1.52 and -1.41 kcal mol⁻¹, whereas for the C₅ position it is endothermic by 2.03 kcal mol⁻¹. The corresponding Gibbs free activation barriers are 13.67, 13.58, and 15.36 kcal mol⁻¹, respectively. Due to the significantly higher activation barriers, these three H-abstraction reactions will not be further discussed. The Gibbs free activation barriers of the hydroxyl radical attacks onto the C₂, C₄, and C₅ atoms *via* pathways 1–3 are 5.31–9.22 kcal mol⁻¹, and the Gibbs reaction energies are from -8.99 to -19.08 kcal mol⁻¹. Particularly, the hydroxyl radical attack onto the C₂ position is the most exothermic ($\Delta H = -28.56$ kcal mol⁻¹), while OH attacks onto the C₅ position have the lowest activation barrier ($\Delta H = -2.97$ kcal mol⁻¹). Evidently, pathways (1–3) have lower barrier heights and are more exothermic compared with pathways (4–6).

3.2. Kinetic analysis

RRKM and TST bimolecular kinetic rate coefficients of the atmospheric reactions between imidazole and OH radicals are listed in Tables 2 and 3 at the pressures of 1 bar and 133 mbar and over the considered temperatures. Further RRKM data computed at higher and lower pressures are shown for the same temperature regimes in Tables S1a–j of the ESI.† Effective rate coefficients [k_{eff}] of the reactions (1)–(3) involve a two-step

Table 2 Kinetic rate constants, effective rate coefficients, and branching ratios for the pathways 1–3 by means of TST and RRKM theory ($x = 2, 3$)

T (K)	Rate constants				Branching ratio (%)				
	IM1 → P1	IMx → P2	IMx → P3	R → P1	R → P2	R → P3	R (1)	R (2)	R (3)
297	1.75×10^9 (4.49×10^8)	3.80×10^7 (4.33×10^7)	4.04×10^{10} (1.57×10^9)	6.61×10^{-14} (1.70×10^{-14})	1.15×10^{-15} (1.31×10^{-15})	1.22×10^{-12} (4.77×10^{-14})	5.12 (25.72)	0.09 (1.99)	94.79 (72.29)
316	2.37×10^9 (5.38×10^8)	6.11×10^7 (6.57×10^7)	4.43×10^{10} (1.55×10^9)	6.88×10^{-14} (1.56×10^{-14})	1.52×10^{-15} (1.64×10^{-15})	1.10×10^{-12} (3.86×10^{-14})	5.87 (27.99)	0.13 (2.93)	94.00 (69.08)
331	2.93×10^9 (6.05×10^8)	8.54×10^7 (8.76×10^7)	4.73×10^{10} (1.53×10^9)	7.11×10^{-14} (1.47×10^{-14})	1.85×10^{-15} (1.90×10^{-15})	1.03×10^{-12} (3.32×10^{-14})	6.46 (29.47)	0.17 (3.83)	93.37 (66.71)
344	3.48×10^9 (6.59×10^8)	1.12×10^8 (1.09×10^8)	4.98×10^{10} (1.50×10^9)	7.32×10^{-14} (1.39×10^{-14})	2.18×10^{-15} (2.14×10^{-15})	9.75×10^{-13} (2.95×10^{-14})	6.97 (30.52)	0.21 (4.71)	92.82 (64.77)
353	3.89×10^9 (6.95×10^8)	1.33×10^8 (1.26×10^8)	5.15×10^{10} (1.49×10^9)	7.49×10^{-14} (1.34×10^{-14})	2.42×10^{-15} (2.30×10^{-15})	9.42×10^{-13} (2.72×10^{-14})	7.34 (31.20)	0.24 (5.37)	92.42 (63.43)
362	4.32×10^9 (7.28×10^8)	1.56×10^8 (1.44×10^8)	5.32×10^{10} (1.47×10^9)	7.64×10^{-14} (1.29×10^{-14})	2.69×10^{-15} (2.47×10^{-15})	9.15×10^{-13} (2.53×10^{-14})	7.69 (31.71)	0.27 (6.08)	92.04 (62.21)
386	5.59×10^9 (8.07×10^8)	2.34×10^8 (1.95×10^8)	5.76×10^{10} (1.42×10^9)	8.40×10^{-14} (1.17×10^{-14})	4.08×10^{-15} (2.90×10^{-15})	8.28×10^{-13} (2.11×10^{-14})	8.61 (32.73)	0.37 (8.12)	91.02 (59.15)
402	6.52×10^9 (8.50×10^8)	2.98×10^8 (2.32×10^8)	6.04×10^{10} (1.39×10^9)	8.40×10^{-14} (1.09×10^{-14})	4.08×10^{-15} (3.19×10^{-15})	8.28×10^{-13} (1.90×10^{-14})	9.16 (33.01)	0.45 (9.61)	90.39 (57.38)
425	7.98×10^9 (9.00×10^8)	4.08×10^8 (2.88×10^8)	6.43×10^{10} (1.34×10^9)	8.89×10^{-14} (1.00×10^{-14})	5.05×10^{-15} (3.57×10^{-15})	7.96×10^{-13} (1.66×10^{-14})	10.00 (33.23)	0.57 (11.82)	89.44 (54.96)
440	8.99×10^9 (9.25×10^8)	4.92×10^8 (3.25×10^8)	6.67×10^{10} (1.31×10^9)	9.24×10^{-14} (9.50×10^{-15})	5.74×10^{-15} (3.79×10^{-15})	7.78×10^{-13} (1.53×10^{-14})	10.54 (33.24)	0.66 (13.28)	88.80 (53.48)

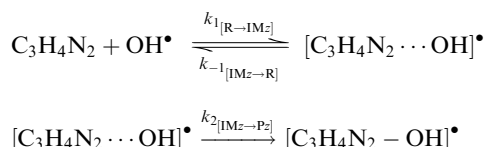
The kinetic parameters in parentheses were calculated at the M06-2X/aug-cc-pVTZ level by means of RRKM theory.



Table 3 Kinetic rate constants, effective rate coefficients, and branching ratios for the pathways **1–3** by means of RRKM ($P = 133$ mbar) ($x = 2,3$)

Rate constants							Branching ratio (%)			
	IM1 → P1	IMx → P2	IMx → P3	R → P1	R → P2	R → P3				
<i>T</i> (K)	k_2 (1) (s ⁻¹)	k_2 (2) (s ⁻¹)	k_2 (3) (s ⁻¹)	k_{eff} (1) (cm ³ mol ⁻¹ s ⁻¹)	k_{eff} (2) (cm ³ mol ⁻¹ s ⁻¹)	k_{eff} (3) (cm ³ mol ⁻¹ s ⁻¹)	R (1)	R (2)	R (3)	$k_{\text{exp}} \times 10^{12,13,15}$ (cm ³ mol ⁻¹ s ⁻¹)
297	7.54×10^7	1.59×10^7	2.14×10^8	2.85×10^{-15}	4.82×10^{-16}	6.49×10^{-15}	29.02	4.91	66.08	(35.9 ± 3.3)
316	8.80×10^7	2.26×10^7	2.11×10^8	2.40×10^{-15}	5.28×10^{-16}	4.93×10^{-15}	30.54	6.72	62.74	(31.1 ± 0.1)
331	9.71×10^7	2.86×10^7	2.07×10^8	2.11×10^{-15}	5.57×10^{-16}	4.03×10^{-15}	31.51	8.32	60.18	(27.3 ± 2.5)
344	1.04×10^8	3.42×10^7	2.04×10^8	1.89×10^{-15}	5.78×10^{-16}	3.45×10^{-15}	31.94	9.77	58.30	(25.2 ± 0.3)
353	1.09×10^8	3.83×10^7	2.01×10^8	1.77×10^{-15}	5.89×10^{-16}	3.09×10^{-15}	32.48	10.81	56.71	(22.5 ± 1.0)
362	1.13×10^8	4.24×10^7	1.99×10^8	1.64×10^{-15}	5.98×10^{-16}	2.81×10^{-15}	32.49	11.85	55.67	(19.8 ± 1.0)
386	1.23×10^8	5.37×10^7	1.92×10^8	1.37×10^{-15}	6.15×10^{-16}	2.20×10^{-15}	32.74	14.70	52.57	(16.3 ± 0.3)
402	1.28×10^8	6.11×10^7	1.87×10^8	1.22×10^{-15}	6.19×10^{-16}	1.89×10^{-15}	32.72	16.60	50.68	(13.9 ± 0.5)
425	1.33×10^8	7.12×10^7	1.80×10^8	1.04×10^{-15}	6.16×10^{-16}	1.56×10^{-15}	32.34	19.15	48.51	(10.4 ± 0.7)
440	1.35×10^8	7.74×10^7	1.76×10^8	9.36×10^{-16}	6.10×10^{-16}	1.39×10^{-15}	31.88	20.78	47.34	(9.1 ± 0.1)

mechanism: at first, a fast and reversible pre-equilibrium between the reactants (R) and the pre-reactive complex **IM** is established, followed by a further irreversible step leading to the related products:



Thus, the effective rate coefficients for the reactions (1)–(3) are given by:

$$k_{\text{eff}}(i) = \frac{k_{\text{R} \rightarrow \text{IMz}} k_{\text{IMz} \rightarrow \text{Pi}}}{k_{\text{IMz} \rightarrow \text{R}} + k_{\text{IMz} \rightarrow \text{Pi}}} \approx K_c(\text{R} \rightleftharpoons \text{IMz}) k_{\text{IMz} \rightarrow \text{Pi}} \quad (7)$$

$$= (RT) \times K_{\text{p}(\text{R} \rightleftharpoons \text{IMz})} k_{\text{IMz} \rightarrow \text{Pi}}; (i = 1 - 3)$$

where $k_{[\text{R} \rightarrow \text{IMz}, (i=1-3)]}$ is the forward rate constant for the first step (in cm³ molecule⁻¹ s⁻¹), while $k_{\text{IMz} \rightarrow \text{P}}$ and $k_{\text{IMz} \rightarrow \text{R}}$ denote the forward and backward unimolecular reaction rate coefficients (in s⁻¹).

A more quantitative insight into the evolution of the regioselectivity for the effective rate coefficients (1)–(3), which is obtained by means of TST and RRKM theories at the pressures of 1.0 bar and 133 mbar and temperatures ranging from 297 to 440 K, is given by:

$$R(i) = k_{\text{eff}}(i) / \sum_{i=1}^3 k_{\text{eff}}(i); (i = 1 - 3) \quad (8)$$

The comparison of the kinetic rate coefficients and branching ratios that have been achieved at the studied temperatures and at a pressure of 1 bar are summarized in Table 2. The main difference is found for the kinetic rate coefficient of the second step in reaction (3) [$k_2(3)$]. Because the pressure issues have to be taken into consideration for a reliable interpretation of the experimental kinetic data, it seems preferable to consider the RRKM approach for evaluating the kinetic rate constant. According to the calculated M06-2X energy profiles and related vibrational frequencies, Wigner tunneling correction $\kappa(T)$ values equal to 1.18, 1.17 and 1.08 were found with TST calculation

for the second reaction step [**IM1 → P1; IMx → P2,P3**] of the pathways **1–3**. These results show that tunneling effects are practically negligible.

As can be seen in Table S2 of the ESI,† because the effective rate coefficient k_r cannot be compared directly with the corresponding k_f [R + OH[•] → P_i; *i* = 1–3], we can treat the 2nd order oxidation reaction as a pseudo 1st order reaction. Using an average hydroxyl radical concentration of 2×10^6 molecule cm⁻³ in the atmosphere,⁵³ apparent kinetic rate constants for forward OH-addition processes, $k_f[\text{OH}]$ are obtained. All reactions (1)–(3) occurring on the C₂, C₄, and C₅ positions indicate that they are reversible processes. Because the $k_f[\text{OH}]$ values are small, their contribution to atmospheric oxidation of imidazole by OH radicals is negligible. The values of k_r are consistently greater than that of $k_f[\text{OH}]$ (see Table S2, ESI†). The obtained results in Table S2 of the ESI,† show that the backward processes of the reactions (1)–(3) are much faster than the forward chemical pathways. Hence, to calculate the possibility of the reactions studied here [reactions (1)–(3)], the subsequent reactions of the corresponding adducts in these reactions should be taken into account.

RRKM estimates for unimolecular (k_2) and effective bimolecular (k_{eff}) kinetic rate coefficients were performed over a temperature range 297–440 K and pressure of 133 mbar and the obtained effective rate coefficients compared with the available experimental data (Table 3).^{13–15} More kinetic data were calculated by means of RRKM theory at higher and lower pressures for the same temperature regimes (summarized in Tables S1a–j of the ESI†).

The Arrhenius plot of the effective rate coefficients for the reaction channels 1–3 using RRKM theory clearly confirms that the formation of **P3** species via OH radical attacks onto the C₅ position will consequently dominate over the formation of the other species (**P1** and **P2**) over a temperature range of 297–440 K and pressure of 133 mbar (see Fig. 4).

The obtained results in Table 3 indicate that RRKM effective rate constants $k_{\text{eff}}(3)$ for reaction (3) are larger by factors 1.49 to 2.28 and 2.28 to 13.46, respectively, than the effective rate constants $k_{\text{eff}}(1)$ and $k_{\text{eff}}(2)$ for reaction pathways **1** and **2**. One can find a similar trend for pressures ranging from 10⁻¹⁰ to 10⁸ bars in Tables S3a–j of the ESI†. Because of the involved



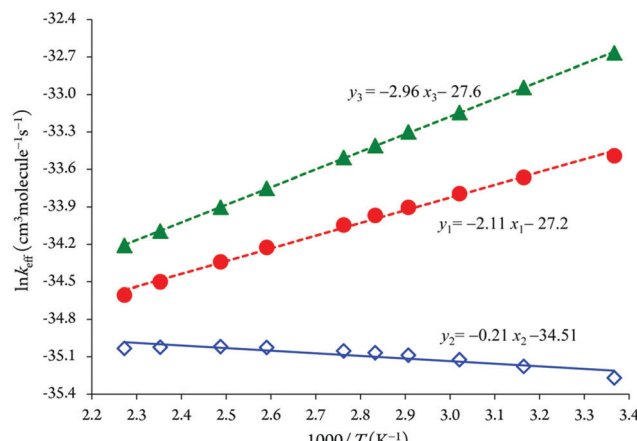


Fig. 4 The Arrhenius plot of the obtained RRKM effective rate coefficients ($P = 133$ mbar). Legend: (●) effective kinetic rates for reaction (1); (◇) effective kinetic rates for reaction (2); (▲) effective kinetic rates for reaction (3).

negative energy barriers for the reactions (1) and (3), the RRKM effective rate coefficients for OH addition onto the C_2 and C_5 positions will decrease gradually with increasing temperatures, while for reaction (2) (OH radical onto the C_4 atom), it is in the opposite manner (see also Tables S1a–j of the ESI[†]). Thus, the reaction channel 3 is a favorable process compared with the reactions (1) and (2) from a kinetic point of view.

It appears that the branching ratios for OH addition onto the C_2 , C_4 and C_5 positions leading to the related energized adducts are predicted as 29.02–32.74%, 4.91–20.78%, and 47.34–66.08%, respectively (see Fig. 5 and Table 3). Branching ratios of the chemical channels 1 and 3 increase gradually with increasing temperatures. In contrast, for the reaction (2) a decrease in the branching ratio is observed. Under atmospheric conditions, the OH addition onto the C_5 position accounts for ~66% of the branching ratio, whereas the remaining ~29% and ~5% for OH addition onto the C_2 and C_4 positions, respectively, are based on the evaluated preceding theoretical results. We remind that the kinetically less efficient reaction is precisely pathway 2, with branching ratios equal to 4.91–20.78% over the temperature range from 297 to 440 K.

We display in Fig. 5 the evolution of branching ratios for the addition of OH attack onto the C_2 , C_4 and C_5 atoms as a function of the temperature and pressure, respectively (see also Table 3 and Tables S3a–j of the ESI,[†] for detailed numerical values at various temperatures ranging from 297 to 440 K, and pressures ranging from 10^{-10} to 10^8 bar). In line with the computed energy profiles and kinetic rate constants (RRKM data), the production of the P3 species (*via* channel 3) clearly dominates over the formation of the P1 and P2 species (*via* channels 1 and 2) at the studied temperatures, down to extremely low pressures, $P > 10^{-10}$ bar. Nevertheless, from these data, and the correspondingly computed regioselectivity indices $\{\text{RSI} = R(3) - [R(1) + R(2)]/[R(1) + R(2) + R(3)]\}$, the regioselectivity of the oxidation process decreases with increasing temperatures and decreasing pressures (see Fig. 6).

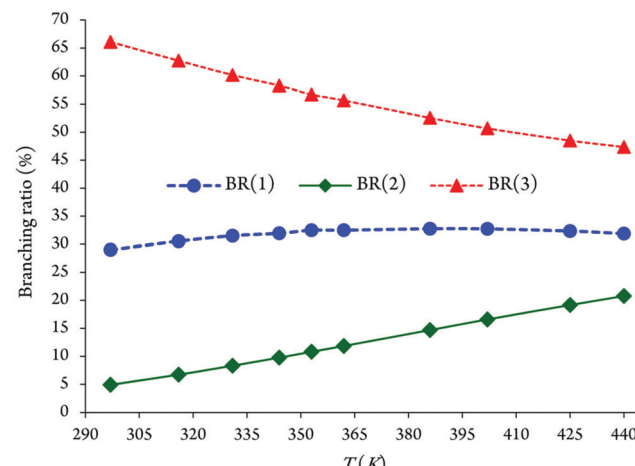


Fig. 5 Evolution of branching ratios as a function of the increasing temperatures for chemical reactions (1)–(3).

The pressure dependence of the calculated effective rate coefficients at 297, 344, 386 and 440 K is shown in Fig. 7. As can be seen in Fig. 7, for ensuring their saturation to the high-pressure limit, pressures $P > 10^2$ bar are required. This observation shows that the calculation of the effective rate constants by means of transition state theory is not valid at atmospheric pressure (1 bar). Hence, pressure effects need to be taken into account on the kinetic study using RRKM theory for consistent insight into the experiment,^{29,33} which was obtained at a pressure of 133 mbar. The obtained RRKM effective rate coefficients related to the reaction (3) are about 2–3 orders of magnitude underestimated. Both the theoretical and experimental rate coefficients for this reaction with increasing temperatures are decreased, which confirms that there is a negative activation energy for this reaction.

3.3. Atmospheric implications

In this study, we used DFT calculations for the chemical reaction (1)–(3) to consider the atmospheric oxidation reaction of imidazole initiated by hydroxyl radicals. The overall TST rate constant for reactions between imidazole with OH radicals at $P = 1$ bar and $T = 297$ K was $1.22 \times 10^{-12} \text{ cm}^3 \text{ molecule}^{-1} \text{ s}^{-1}$. The obtained kinetic rate coefficient can be applied to measure the lifetime for imidazole under the atmospheric conditions. Assuming typical tropospheric 12 h daytime average concentrations of OH radicals as $2 \times 10^6 \text{ molecule cm}^{-3}$,⁵³ the lifetime of imidazole relative to reaction with hydroxyl radicals is calculated to be ~4.74 days which suggests imidazole can contribute to the formation of various secondary pollutants like ozone, peroxyacetyl nitrates (PANs), and nitric acid following emission into the atmosphere.

3.4. Natural bond orbital analysis

Natural bond orbital analysis was initially established as a way of quantifying resonance structure contributions to molecular systems. The energetic stabilizations are taken into account for all possible interactions between “filled” (donor) Lewis-type NBOs and “empty” (acceptor) non-Lewis NBOs and then their



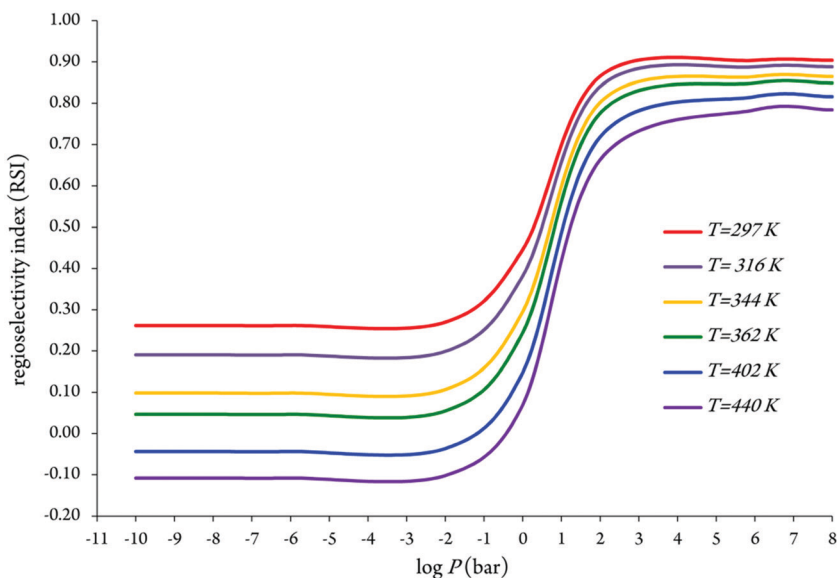


Fig. 6 Temperature and pressure dependence of the regioselectivity in the oxidation of imidazole by OH radicals based on the obtained effective rate constants [$k_{\text{eff}}(\mathbf{1})$, $k_{\text{eff}}(\mathbf{2})$, and $k_{\text{eff}}(\mathbf{3})$] by means of RRKM theory.

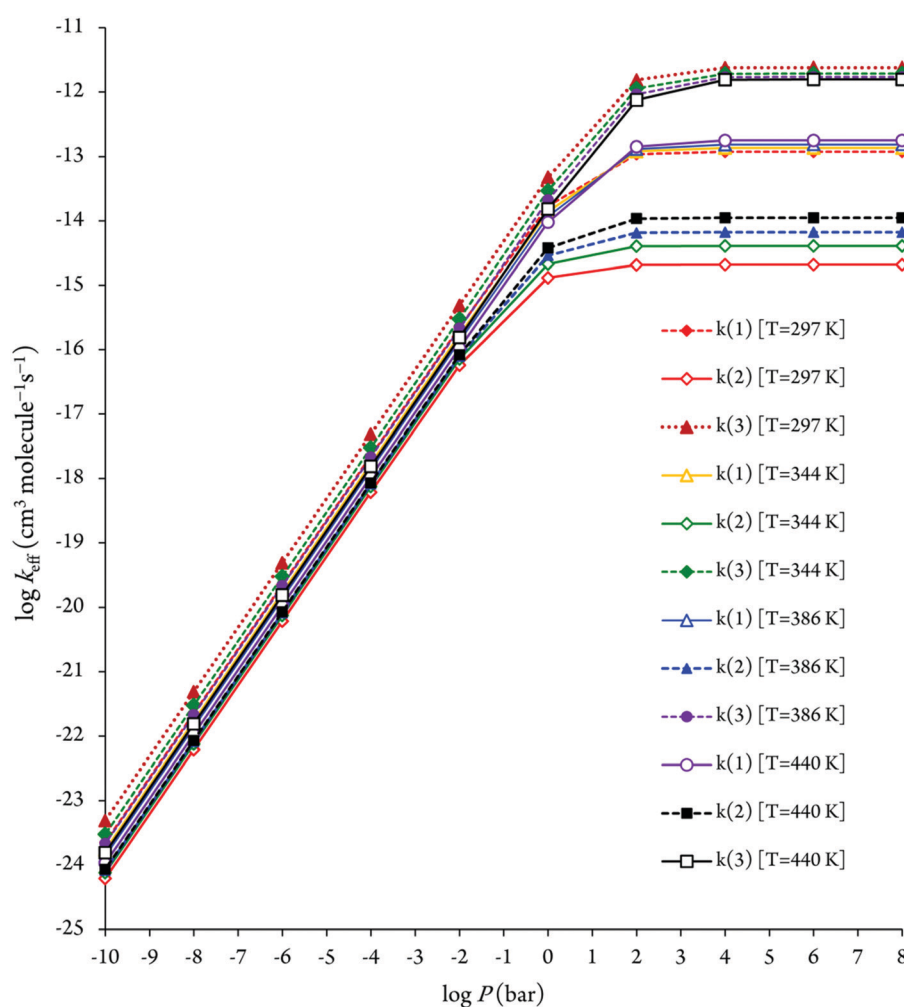


Fig. 7 Pressure dependence of the RRKM bimolecular rate constants for the pathways **1-3**.



energies are estimated by 2nd-order perturbation theory.⁵⁴ Delocalization energy (E_2) for each donor NBO(i) and acceptor NBO(j) is given by:⁵⁵

$$E_2 = \Delta E_{ij} = q_i \left[\frac{F_{(i,j)}^2}{\varepsilon_i - \varepsilon_j} \right] \quad (9)$$

where ε_i and ε_j represent diagonal matrixes of orbital energies, $F_{(i,j)}$ denotes the off-diagonal NBO Fock matrix elements, and q_i is the donor orbital occupancy.

Based on the optimized geometries of the 2-hydroxyimidazolyl radical (**P1**) and 5-hydroxyimidazolyl (**P3**) radical, the natural bond orbital analysis demonstrates that the delocalization energies related to the electron delocalization from the non-bonding nitrogen lone pair orbital LP(1)N₁ to $\sigma^*(C_4-C_5)$ antibonding orbitals are equal to 4.58 and 4.61 kcal mol⁻¹, respectively. Furthermore, NBO analysis shows that the $\sigma(C_4-C_5)$ bonding orbital occupancies for energized adducts **P1** and **P3** are both equal to ~ 0.994 , whereas the $\sigma^*(C_4-C_5)$ antibonding orbital occupancies in the energized adducts **P1** and **P3** are equal to ~ 0.040 and ~ 0.022 , respectively.

Table 4 shows that for the transition states **TS1** and **TS3**, strong interaction prevails between one nitrogen lone pair of imidazole and the unoccupied $\pi^*(C_4-C_5)$ orbital, resulting for the latter orbital in occupancies around 0.157 and 0.167, respectively. The delocalization energies for **TS1** and **TS3** are equal to 20.31 and 27.12 kcal mol⁻¹, respectively. Moreover, charge transfer delocalization donates the larger stability of the **TS3** (OH attack onto C₅ atom) compared with the **TS1** (OH attack onto C₂ atom). NBO analysis demonstrates that, compared with imidazole, the LP(1)N₁ \rightarrow $\pi^*(C_4-C_5)$ delocalization energies have a strong effect on the energy barriers which was computed for pathway 1 ($E_2 = 20.31$ kcal mol⁻¹) and pathway 3 ($E_2 = 27.12$ kcal mol⁻¹). The occupancies of the $\pi(C_4-C_5)$ bonding orbital in the transition states **TS1** and **TS3** amount to 0.948 and 0.911, respectively, whereas the occupancies of $\pi^*(C_4-C_5)$ antibonding orbitals in these structures are equal to 0.157 and 0.167, respectively. Furthermore, the NBO data for the transition states **TS1** and **TS3** show that a slight interaction prevails between one of the nitrogen lone pairs of imidazole and the unoccupied $\sigma^*(C_4-C_5)$ orbital, resulting for the latter orbital in an occupancy around 0.011. The corresponding stabilization

energies for **TS1** and **TS3** are equal to 3.68 and 3.88 kcal mol⁻¹, respectively.

4. Conclusions

The atmospheric oxidation mechanisms of imidazole initiated by hydroxyl radicals *via* OH-addition and H-abstraction processes were studied for the first time at the M06-2X/aug-cc-pVTZ level of theory. The difference in reaction energies shows that the production of species related to the OH-addition process will be thermodynamically favorable, and these reactions seem to be strongly exothermic reactions. This first reaction step for OH addition onto the different carbon positions was found to be an exoergic process ($\Delta G < 0$) at ambient temperature and pressure. In line with the experiment, due to the formation of a prereactive complex [C₃H₄N₂ · · OH][•], the corresponding transition state lies below the isolated reactant; therefore, effective negative activation energies around -1.53 and -2.97 kcal mol⁻¹ are related to the OH radical attacks onto the C₂ and C₅ positions, respectively.

Kinetic rate coefficients for unimolecular and bimolecular reaction steps were estimated by means of transition state theory and Rice–Ramsperger–Kassel–Marcus theory. Effective rate coefficients involve a two-step mechanism: at first, a fast and reversible pre-equilibrium between the isolated reactants (imidazole and OH radicals) and the pre-reactive complex [C₃H₄N₂ · · OH][•] is established, followed by a further irreversible step leading to the related products. In proportion to the experiment, the obtained branching ratios show that the kinetically most efficient process over the temperature range 297–440 K correspond to OH addition onto a carbon atom which is adjacent to the nitrogen atom having a lower energy barrier. These ratios also reveal that the regioselectivity of the oxidation reaction decreases with increasing temperatures and decreasing pressures.

A comparison with TST results seems to validate RRKM theory for all OH additions onto different carbon atoms of imidazole (C₂, C₄, and C₅ positions). The obtained RRKM effective rate coefficients for the favorable reaction appear to be sufficient for achieving semi-quantitative insights into the available experimental kinetic data with discrepancies, which are about 2–3 orders of magnitude underestimated. The theoretical rate coefficient for the favorable reaction shows that it decreases with increasing temperatures, which confirms that there is a negative activation energy.

In line with negative activation energies, it was found that the standard transition-state-approximation breaks down at ambient pressure for the first bimolecular reaction steps. RRKM calculations reveal that overwhelmingly high pressures, where $P > 10^2$ bar, are required to ensure the validity of the transition state theory approximation for the OH addition onto all carbon position pathways.

NICS indices and natural bond orbital analysis show that the computed activation energies are dictated by charge transfer effects and aromaticity changes because of the delocalization of nitrogen lone pairs to neighboring empty π^* orbitals.

Table 4 Delocalization energies (in kcal mol⁻¹) and natural bond orbital occupancies of transition states and products along the reactions (1) and (3)

	Imidazole	TS1	TS3	P1	P3
Occupancies					
$\sigma(C_4-C_5)$	0.99369	0.99388	0.99363	0.99300	0.99361
$\pi(C_4-C_5)$	0.92975	0.94807	0.91073	0.98827	0.82432
LP(1)N ₁	0.79424	0.80502	0.78782	0.93083	0.90059
LP(1)N ₃	0.96186	0.96280	0.96233	0.96419	0.96009
$\sigma^*(C_4-C_5)$	0.01014	0.01078	0.01091	0.03945	0.02207
$\pi^*(C_4-C_5)$	0.14731	0.15739	0.16649	0.16680	0.19802
Stabilization energies (E_2)					
LP(1)N ₁ \rightarrow $\pi^*(C_4-C_5)$	20.68	20.31	27.12	9.01	4.45
LP(1)N ₃ \rightarrow $\sigma^*(C_4-C_5)$	3.50	3.88	3.68	4.58	4.61



Conflicts of interest

There are no conflicts to declare.

Acknowledgements

Funding by Maa-ja vesitekniikan tuki ry (MVTT) is acknowledged. The authors would also like to acknowledge the contributions of Environics OY.

References

- 1 A. L. Lehninger, D. L. Nelson and M. M. Cox, *Principles of Biochemistry*, Worth Publishers, New York, 1993.
- 2 L. Stryer, *Biochemistry*, Freeman & Company, New York, 2nd edn, 1981.
- 3 J. Llano and L. A. Eriksson, Mechanism of hydroxyl radical addition to imidazole and subsequent water elimination, *J. Phys. Chem. B*, 1999, **103**, 5598–5607.
- 4 R. A. Perry, R. Atkinson and J. N. Pitts Jr, Kinetics and mechanism of the gas phase reaction of hydroxyl radicals with aromatic hydrocarbons over the temperature range 296–473 K, *J. Phys. Chem.*, 1977, **81**, 296–304.
- 5 D. Martin, J. L. Jourdain and G. Le Bras, Kinetic study for the reactions of OH radicals with dimethylsulfide, diethylsulfide, tetrahydrothiophene, and thiophene, *Int. J. Chem. Kinet.*, 1985, **17**, 1247–1261.
- 6 P. H. Wine and R. J. Thompson, Kinetics of OH reactions with furan, thiophene, and tetrahydrothiophene, *Int. J. Chem. Kinet.*, 1984, **16**, 867–878.
- 7 R. Atkinson, S. M. Aschmann and W. P. L. Carter, Kinetics of the reactions of O₃ and OH radicals with furan and thiophene at 298 ± 2 K, *Int. J. Chem. Kinet.*, 1983, **15**, 51–61.
- 8 H. MacLeod, J. L. Jourdain and G. Le Bras, Absolute rate constant for the reaction of OH with thiophene between 293 and 473 K, *Chem. Phys. Lett.*, 1983, **98**, 381–385.
- 9 J. H. Lee and I. N. Tang, Absolute rate constants for the hydroxyl radical reactions with ethane, furan, and thiophene at room temperature, *J. Chem. Phys.*, 1982, **77**, 4459–4463.
- 10 T. J. Wallington, Kinetics of the gas phase reaction of OH radicals with pyrrole and thiophene, *Int. J. Chem. Kinet.*, 1986, **18**, 487–496.
- 11 E. C. Tuazon, R. Atkinson, A. M. Winer and J. N. Pitts Jr., A study of the atmospheric reactions of 1,3-dichloropropene and other selected organochlorine compounds, *Arch. Environ. Contam. Toxicol.*, 1984, **13**, 691–700.
- 12 R. Atkinson, S. M. Aschmann, A. M. Winer and W. P. L. Carter, Rate constants for the gas phase reactions of OH radicals and O₃ with pyrrole at 295 ± 1 K and atmospheric pressure, *Atmos. Environ.*, 1984, **18**, 2105–2107.
- 13 F. Witte and C. Zetzsch, Examination of the temperature dependence for the reaction of OH radicals with heterocyclic aromatics (imidazole, furan, pyrrole and thiophene) and the unimolecular decay of the adducts imidazole-OH and thiophene-OH, 9th International Symposium on Gas Kinetics, University of Bordeaux, Bordeaux, France, 1986.
- 14 R. Atkinson, Kinetic and mechanism of the gas-phase reactions of the hydroxyl radical with organic compounds under atmospheric conditions, *Chem. Rev.*, 1985, **85**, 69–201.
- 15 R. Atkinson, Kinetics and mechanisms of the gas-phase reactions of the hydroxyl with organic compounds, *J. Phys. Chem. Ref. Data, Monogr.*, 1989, **1**, 1–246.
- 16 D. Lucas and N. J. Brown, The influence of thiophene on the selective reduction of NO by NH₃, *Combust. Flame*, 1983, **49**, 283–288.
- 17 A. Samuni and P. Neta, Electron spin resonance study of the reaction of hydroxyl radicals with pyrrole, imidazole, and related compounds, *J. Phys. Chem.*, 1973, **77**, 1629–1635.
- 18 G. Lassmann, L. A. Eriksson, F. Himo, F. Lendzian and W. Lubitz, Electronic structure of a transient histidine radical in liquid aqueous solution: EPR continuous-flow studies and density functional calculations, *J. Phys. Chem. A*, 1999, **103**, 1283–1290.
- 19 L. A. Eriksson and F. Himo, Radicals in biophysical systems—A theoretical perspective, *Trends Phys. Chem.*, 1997, **6**, 153–170.
- 20 P. Cysewski, An *ab initio* study on nucleic acid bases aromaticities, *THEOCHEM*, 2005, **714**, 29–34.
- 21 P. v. R. Schleyer, C. Maerker, A. Dransfeld, H. Jiao and N. J. R. van Eikema Hommes, Nucleus-independent chemical shifts: a simple and efficient aromaticity probe, *J. Am. Chem. Soc.*, 1996, **118**, 6317–6318.
- 22 S. Nigam, C. Majumder and S. K. Kulshreshtha, Theoretical study of aromaticity in inorganic tetramer clusters, *J. Chem. Sci.*, 2006, **118**, 575–578.
- 23 P. v. R. Schleyer, M. Manoharan, Z. X. Wang, B. Kiran, H. J. Jiao, R. Puchta and N. Hommes, Dissected nucleus-independent chemical shift analysis of π-aromaticity and antiaromaticity, *Org. Lett.*, 2001, **3**, 2465–2468.
- 24 P. v. R. Schleyer, H. Jiao, B. Goldfuss and P. K. Freeman, Aromaticity and antiaromaticity in five-membered C₄H₄X ring systems: “classical” and “magnetic” concepts may not be “orthogonal”, *Angew. Chem. Int. Ed. Engl.*, 1995, **34**, 337–340.
- 25 A. E. Reed, R. B. Weinstock and F. Weinhold, Natural population analysis, *J. Chem. Phys.*, 1985, **83**, 735–746.
- 26 J. K. Badenhoop and F. Weinhold, Natural steric analysis of internal rotation barriers, *Int. J. Quantum Chem.*, 1999, **72**, 269–280.
- 27 M. J. Frisch, G. W. Trucks, H. B. Schlegel, G. E. Scuseria, M. A. Robb, J. R. Cheeseman, G. Scalmani, V. Barone, B. Mennucci, G. A. Petersson, *et al.*, *Gaussian 09, Revision B.01*, Gaussian, Wallingford, CT, 2009.
- 28 Y. Zhao and D. G. Truhlar, Density functionals with broad applicability in chemistry, *Acc. Chem. Res.*, 2008, **41**, 157–167.
- 29 Y. Zhao and D. G. Truhlar, The M06 suite of density functionals for main group thermochemistry, thermochemical kinetics, noncovalent interactions, excited states, and transition elements: two new functionals and systematic testing of four M06-class functionals and 12 other functionals, *Theor. Chem. Acc.*, 2008, **120**, 215–241.
- 30 J. P. Merrick, D. Moran and L. Radom, An evaluation of harmonic vibrational frequency scale factors, *J. Phys. Chem. A*, 2007, **111**, 11683–11700.



31 F. Fukui, A formulation of the reaction coordinate, *J. Phys. Chem.*, 1970, **74**, 4161–4163.

32 Z. Safaei, A. Shiroudi, R. Padash, M. Sillanpää and E. Zahedi, Reaction mechanisms and kinetics of the β -elimination processes of compounds $\text{CHF}_2\text{CH}_2\text{SiF}_n\text{Me}_{3-n}$ ($n = 0\text{--}3$): DFT and CBS-QB3 methods using Rice–Ramsperger–Kassel–Marcus and transition state theories, *J. Fluorine Chem.*, 2018, **216**, 71–80.

33 K. Wolinski, J. F. Hilton and P. Pulay, Efficient implementation of the gauge-independent atomic orbital method for NMR chemical shift calculations, *J. Am. Chem. Soc.*, 1990, **112**, 8251–8260.

34 R. F. W. Bader, *Atoms in Molecules: A Quantum Theory*, Clarendon, Oxford, 1990.

35 F. P. Cossío, I. Morao, H. J. Jiao and P. v. R. Schleyer, In-plane aromaticity in 1,3-dipolar cycloadditions. Solvent effects, selectivity, and nucleus-independent chemical shifts, *J. Am. Chem. Soc.*, 1999, **121**, 6737–6746.

36 I. Morao, B. Lecea and F. P. Cossío, In-plane aromaticity in 1,3-dipolar cycloadditions, *J. Org. Chem.*, 1997, **62**, 7033–7036.

37 D. L. Singleton and R. J. Cvetanovic, Temperature dependence of the reaction of oxygen atoms with olefins, *J. Am. Chem. Soc.*, 1976, **98**, 6812–6819.

38 J. R. Alvarez-Idaboy, N. M. Diez and A. Vivier-Bunge, A quantum chemical and classical transition state theory explanation of negative activation energies in OH addition to substituted ethenes, *J. Am. Chem. Soc.*, 2000, **122**, 3715–3720.

39 V. H. Uc, J. R. Alvarez-Idaboy, A. Galano and A. Vivier-Bunge, Theoretical explanation of nonexponential OH decay in reactions with benzene and toluene under pseudo-first-order conditions, *J. Phys. Chem. A*, 2008, **112**, 7608–7615.

40 E. Wigner, Calculation of the rate of elementary association reactions, *J. Chem. Phys.*, 1937, **5**, 720–725.

41 E. P. Wigner, Über das überschreiten von potentialschwellen bei chemischen reaktionen, *Z. Phys. Chem., Abt. B*, 1932, **19**, 203–216.

42 K. A. Holbrook, M. J. Pilling, S. H. Robertson and P. J. Robinson, *Unimolecular Reactions*, Wiley, New York, 2nd edn, 1996.

43 M. J. Pilling and P. W. Seakins, *Reaction Kinetics*, Oxford University Press Inc., New York, 1999.

44 D. R. Glowacki, L. Wang and M. J. Pilling, Evidence of Formation of Bicyclic Species in the Early Stages of Atmospheric Benzene Oxidation, *J. Phys. Chem. A*, 2009, **113**, 5385–5396.

45 R. G. Gilbert and S. C. Smith, *Theory of Unimolecular and Recombination Reactions*, Blackwell Scientific Publications, Boston, MA, 1990.

46 S. Canneaux, F. Bohr and E. Henon, KiSTheLP: a program to predict thermodynamic properties and rate constants from quantum chemistry results, *J. Comput. Chem.*, 2013, **35**, 82–93.

47 Computational chemistry comparison and benchmark database, precomputed vibrational scaling factors. (<http://cccbdb.nist.gov/vibscalejust.asp>).

48 R. J. Kee, F. M. Rupley, J. A. Miller, M. E. Coltrin, J. F. Grar, E. Meeks, H. K. Moffat, A. E. Lutz, G. Dixon-Lewis, M. D. Smooke, J. Warnatz, G. H. Evans, R. S. Larson, R. E. Mitchell, L. R. Petzold, W. C. Reynolds, M. Caracotsios, W. E. Stewart, P. Glarborg, C. Wang, C. L. McLellan, O. Adigun, W. G. Houf, C. P. Chou, S. F. Miller, P. Ho, P. D. Young, D. J. Young, D. W. Hodgson, M. V. Petrova and K. V. Puduppakkam, *Chemkin, Reaction design*, San Diego, California, 2010.

49 F. M. Mourits and H. A. Rummens, A critical evaluation of Lennard-Jones and Stockmayer potential parameters and of some correlation methods, *Can. J. Chem.*, 1977, **55**, 3007–3020.

50 J. R. Alvarez-Idaboy, N. Mora-Diez, R. J. Boyd and A. Vivier-Bunge, On the importance of prereactive complexes in molecule-radical reactions: hydrogen abstraction from aldehydes by OH, *J. Am. Chem. Soc.*, 2001, **123**, 2018–2024.

51 C. W. Zhou, A. M. Mebel and X. Y. Li, An ab initio/Rice–Ramsperger–Kassel–Marcus study of the reactions of propenols with OH. Mechanism and kinetics of H abstraction channels, *J. Phys. Chem. A*, 2009, **113**, 10667–10677.

52 G. S. Hammond, A correlation of reaction rates, *J. Am. Chem. Soc.*, 1953, **77**, 334–338.

53 R. G. Prinn, R. F. Weiss, B. R. Miller, J. Huang, F. N. Alyea, D. M. Cunnold, P. J. Fraser, D. E. Hartley and P. G. Simmonds, Atmospheric trends and lifetime of CH_3CCl_3 and global OH concerns, *Science*, 1995, **269**, 187–192.

54 J. E. Carpenter and F. Weinhold, Analysis of the geometry of the hydroxymethyl radical by the different hybrids for different spins natural bond orbital procedure, *THEOCHEM*, 1988, **169**, 41–62.

55 A. E. Reed, L. A. Curtiss and F. Weinhold, Intermolecular interactions from a natural bond orbital, donor–acceptor viewpoint, *Chem. Rev.*, 1988, **88**, 899–926.

